JPE 18-4-6

https://doi.org/10.6113/JPE.2018.18.4.1007
ISSN(Print): 1598-2092 / ISSN(Online): 2093-4718

Novel Dual DC-DC Flyback Converter with Leakage-Energy Recycling

Lung-Sheng Yang†

†Department of Electrical Engineering, Far East University, Tainan, Taiwan

Abstract

A novel dual DC-DC flyback converter with leakage-energy recycling is presented in this paper. Only an active switch is used for this converter. A pulse-width-modulation strategy is adopeted to control this switch. Two transformers are employed for the proposed converter. During the switch ON-period, the primary windings of the two transformers store energies. At the switch OFF-period, the energies stored in the primary windings of the two transformers are released to the output via the secondary windings of the two transformers. Meanwhile, the leakage energies of the two transformers can be recycled. The operating principles and steady-state analyses of the proposed converter are described in detail. A prototype circuit of the proposed converter is implemented for verifying the performances.

Key words: Flyback converter, Leakage-energy recycling, Pulse width modulation

I. INTRODUCTION

DC power sources are widely utilized in many products, such as communication equipment, medical instruments, and both industrial and commercial devices. It includes nearly all electronics products. Switching mode power converters are applied to the DC power sources. High switching frequencies are used for these converters. Therefore, these converters can provide a high power density, high stability, fast regulation etc. Many topologies, including buck converters [1]-[3], boost converters [4]-[6], buck-boost converters [7], [8], Cuk converters [9], [10] and SEPIC converters [11], [12], have been researched for non-isolated applications. For isolated applications, the forward and flyback converters are used for low-power applications [13]-[18]. In addition, half-bridge, full-bridge and push-pull converters have been utilized for high-power applications [19]-[24]. For isolated and low-power applications, flyback converters are attractive due to their simple structure and low cost. However, the main drawback of flyback converters is the existence of leakage inductance of the transformer. It results in a high voltage spike on the active switch and high power losses. In order to improve this problem, some techniques have been studied. An RCD snubber has been used to limit the voltage spikes on the active switches [25]. However, the energy stored in the leakage inductance of the transformer is dissipated into the resistor of the RCD snubber. A two-switch flyback converter has been used to recycle the leakage-energy of transformers [26], [27]. Nevertheless, this topology need two active switches, which results in higher costs. An active clamp circuit has been applied to eliminate the voltage spike on active switches [28], [29]. In addition, this converter can provide zero voltage switching for the active switch. However, two active switches are employed for this converter. The interleaved flyback converter employs two transformers for high power applications [30]. The leakage energies of the two transformers can be recycled. However, two active switches are employed for this converter as well.

In this paper, a novel single switch dual DC-DC flyback converter with leakage-energy recycling is presented. The circuit configuration of the proposed converter is displayed in Fig. 1. The proposed converter is composed of one switch S_1, two transformers TR_1 and TR_2, three diodes D_1, D_2 and D_3, and three capacitors C_1, C_2 and C_o. The windings in the transformers TR_1 and TR_2 have same turns, $N_{11} = N_{21}$ and $N_{12} = N_{22}$, and turns ratios $n = N_{12} / N_{11} = N_{22} / N_{21}$. The leakage energies of the transformers TR_1 and TR_2 can be recycled into the capacitors C_1 and C_2 via the diode D_1 at the switch S_1 OFF-period. Therefore, the power losses can be reduced. For

Manuscript received Oct. 2, 2017; accepted Feb. 26, 2018
Recommended for publication by Associate Editor Yan Xing.
†Corresponding Author: yanglungsheng@yahoo.com.tw
Tel: +886-6-5979566-5410, Far East University
Dept. of Electric Eng., Far East University, Taiwan

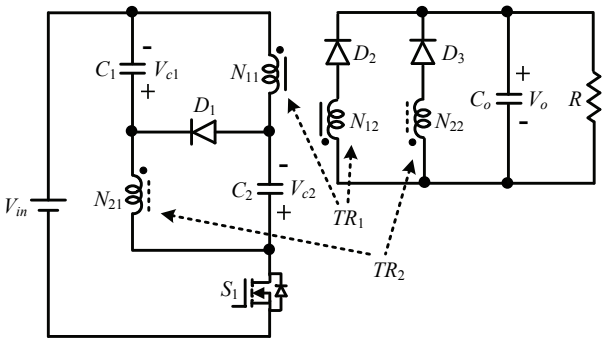

Fig. 1. Circuit configuration of the proposed converter.

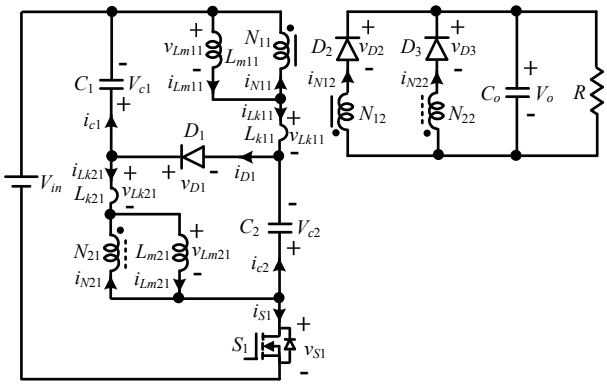

Fig. 2. Equivalent circuit of the proposed converter.

simplifying the circuit analysis of the proposed converter, it is assumed that all of the components are ideal. Therefore, the conducting resistance of the active switch S_1, the forward voltage drop of the diodes D_1, D_2 and D_3, the equivalent series resistance (ESR) of the transformers TR_1 and TR_2 and capacitors C_1, C_2 and C_o are ignored. In addition, these capacitors are sufficiently large. The voltages across these capacitors are considered constant at each switching period.

II. Operating Principle

An equivalent circuit of the proposed converter is displayed in Fig. 2. The active switch S_1 is controlled by utilizing the pulse-width modulation strategy. The transformer TR_1 is modeled as the magnetizing inductance L_{m11}, the leakage inductance L_{k11}, and an ideal transformer. Similarly, the transformer TR_2 is modeled as the magnetizing inductance L_{m21}, the leakage inductance L_{k21} and an ideal transformer. Because the windings of the transformers TR_1 and TR_2 have same turns, the magnetizing-inductance and leakage-inductance of the transformers TR_1 and TR_2 are assumed as follows:

$$L_{m11} = L_{m21} = L_m \tag{1}$$

$$L_{k11} = L_{k21} = L_k \tag{2}$$

The coupling coefficient k of the transformers TR_1 and TR_2 is given as:

$$k = \frac{L_m}{L_m + L_k} \tag{3}$$

Some typical waveforms during one switching period in continuous conduction mode (CCM) operation are displayed in Fig. 3. In addition, the equations are assumed as:

$$i_{Lm11} = i_{Lm21} = i_{Lm} \tag{4}$$

$$v_{Lm11} = v_{Lm21} = v_{Lm} \tag{5}$$

$$i_{Lk11} = i_{Lk21} = i_{Lk} \tag{6}$$

$$v_{Lk11} = v_{Lk21} = v_{Lk} \tag{7}$$

$$V_{c1} = V_{c2} = V_c \tag{8}$$

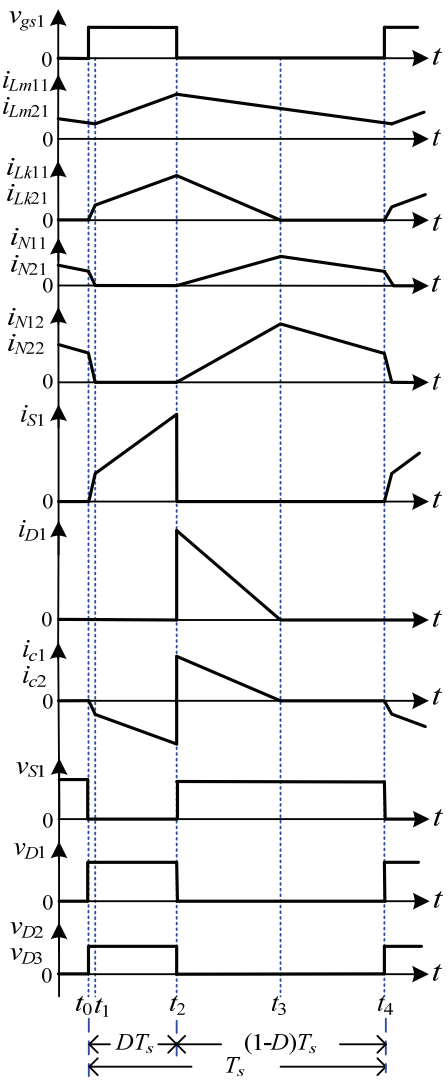

Fig. 3. Some typical waveforms during one switching period of the proposed converter.

The operating principles in CCM operation are described as follows.

Mode I [t_0, t_1]: The active switch S_1 is turned on. The current direction is displayed in Fig. 4(a). The energies stored

in the magnetizing inductances L_{m11} and L_{m21} of the transformers are released to the output capacitor C_o and the load R via ideal transformers and the diodes D_2 and D_3. The DC-source V_{in}, the capacitor C_1 and the magnetizing inductance L_{m21} transfer their energies to the leakage inductance L_{k21} in series via the active switch S_1. Similarly, the DC-source V_{in}, the magnetizing inductance L_{m11} and the capacitor C_2 transfer their energies to the leakage inductance L_{k11} in series via the active switch S_1. Thus, the magnetizing-inductance currents i_{Lm11} and i_{Lm21} are decreased and the leakage-inductance currents i_{Lk11} and i_{Lk21} are increased, as displayed in Fig. 3. This mode ends when the magnetizing-inductance currents i_{Lm11} and i_{Lm21} are equal to the leakage-inductance currents i_{Lk11} and i_{Lk21} at the moment $t = t_1$. The voltages across the magnetizing inductances L_{m11} and L_{m21} and the leakage inductances L_{k11} and L_{k21} are found as follows:

$$v_{Lm}^{I} = -\frac{V_o}{n} \tag{9}$$

$$v_{Lk}^{I} = V_{in} + V_c + \frac{V_o}{n} \tag{10}$$

From the above equations, the currents through the magnetizing inductances L_{m11} and L_{m21} and the leakage inductances L_{k11} and L_{k21} are derived as:

$$i_{Lm}^{I}(t) = -\frac{V_o}{nL_m}(t - t_0) + i_{Lm}(t_0) \tag{11}$$

$$i_{Lk}^{I}(t) = \frac{1}{L_k}(V_{in} + V_c + \frac{V_o}{n})(t - t_0) \tag{12}$$

Mode II [t_1, t_2]: The active switch S_1 is still turned on. The current direction is displayed in Fig. 4(b). The DC-source V_{in} and the capacitor C_1 are in series to transfer their energies for the magnetizing inductance L_{m21} and the leakage inductance L_{k21} via the active switch S_1. Similarly, the DC-source V_{in} and the capacitor C_2 are in series to transfer their energies for the magnetizing inductance L_{m11} and the leakage inductance L_{k11} via the active switch S_1. The energy stored in the output capacitor C_o is discharged to the load R. Therefore, the magnetizing-inductance currents i_{Lm11} and i_{Lm21}, and the leakage-inductance currents i_{Lk11} are i_{Lk21} are increased, as displayed in Fig. 3. This mode ends when the active switch S_1 is turned off at this moment $t = t_2$. The following equations are given as:

$$v_{Lm}^{II} + v_{Lk}^{II} = V_{in} + V_c \tag{13}$$

$$i_{Lm}^{II} = i_{Lk}^{II} \tag{14}$$

Owing to:

$$v_{Lk}^{II} = L_k \frac{di_{Lk}^{II}}{dt} = \frac{1-k}{k} L_m \frac{di_{Lm}^{II}}{dt} \tag{15}$$

The voltage v_{Lk} is rewritten as:

$$v_{Lk}^{II} = \frac{1-k}{k} v_{Lm}^{II} \tag{16}$$

Substituting (16) into (13) yields:

$$v_{Lm}^{II} = k(V_{in} + V_c) \tag{17}$$

Using (12) and (20), the current i_{Lm} is derived as:

$$i_{Lm}^{II}(t) = \frac{k(V_{in} + V_c)}{L_m}(t - t_1) + i_{Lm}(t_1) \tag{18}$$

Mode III [t_2, t_3]: The active switch S_1 is turned off. The current direction is displayed in Fig. 4(c). The magnetizing inductance L_{m21} and the leakage inductance L_{k21} are in series to release their energies to the capacitor C_2 via the diode D_1. Similarly, the magnetizing inductance L_{m11} and the leakage inductance L_{k11} are series to release their energies to the capacitor C_1 via the diode D_1. Thus, the leakage energies have been recycled. The energies stored in the magnetizing inductances L_{m11} and L_{m21} are released to the load R via ideal transformers and the diodes D_2 and D_3. The energy of the output capacitor C_o is also discharged to the load R. Therefore, the magnetizing-inductance currents i_{Lm11} and i_{Lm21} and the leakage-inductance currents i_{Lk11} and i_{Lk21} are decreased, as displayed in Fig. 3. This mode ends when the leakage-inductance currents i_{Lk11} and i_{Lk21} are equal to zero at this moment $t = t_3$. The voltages across the magnetizing inductances L_{m11} and L_{m21}, and the leakage inductances L_{k11} and L_{k21} are obtained as follows:

$$v_{Lm}^{III} = -\frac{V_o}{n} \tag{19}$$

$$v_{Lk}^{III} = \frac{V_o}{n} - V_c \tag{20}$$

Thus:

$$i_{Lm}^{III}(t) = -\frac{V_o}{nL_m}(t - t_2) + i_{Lm}^{II}(t_2) \tag{21}$$

$$i_{Lk}^{III}(t) = \frac{1}{L_k}(\frac{V_o}{n} - V_c)(t - t_2) + i_{Lk}^{II}(t_2) \tag{22}$$

Mode IV [t_3, t_4]: The active switch S_1 is still turned off. The current direction is displayed in Fig. 4(d). The energies stored in the magnetizing inductances L_{m11} and L_{m21} are released to the output capacitor C_o and the load R via ideal transformers and the diodes D_2 and D_3. Thus, the magnetizing-inductance currents i_{Lm11} and i_{Lm21} are decreased, as displayed in Fig. 3. This mode ends when the active switch S_1 is turned on at the beginning of the next switching period. The voltages across the magnetizing inductances L_{m11} and L_{m21} are found as follows:

$$v_{Lm}^{IV} = -\frac{V_o}{n} \tag{23}$$

In additon:

$$i_{Lm}^{IV}(t) = -\frac{V_o}{nL_m}(t - t_3) + i_{Lm}^{III}(t_3) \tag{24}$$

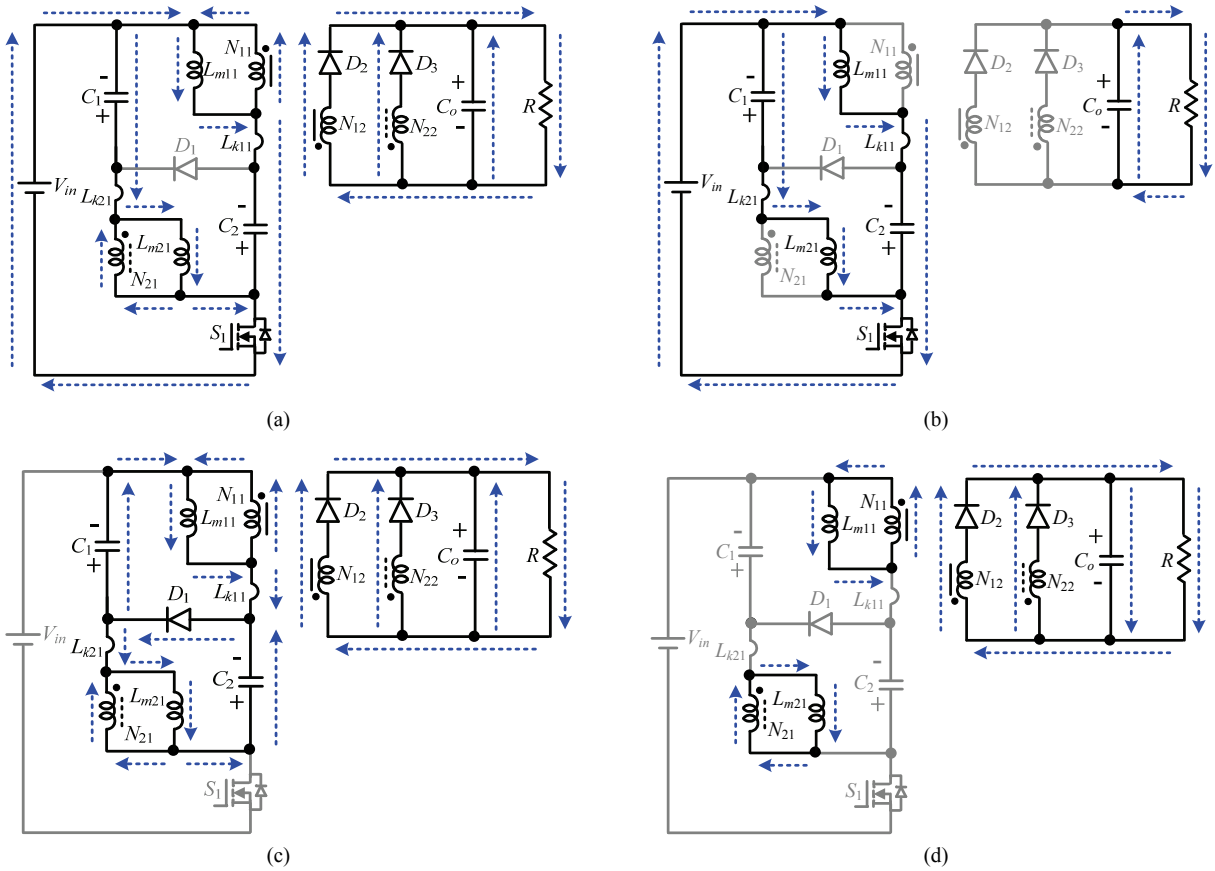

Fig. 4. Current direction of the proposed converter: (a) Mode I; (b) Mode II; (c) Mode III; (d) Mode IV.

III. Steady-State Analysis

A. Voltage Gain

Since the time durations of mode I are very short when compared to a switching period, mode I is neglected in the following analysis. By using the voltage-second balance principle for the magnetizing inductance L_{m11}, the following equation is given as:

$$v_{Lm}^{II}DT_s + v_{Lm}^{III}(t_3 - t_2) + v_{Lm}^{IV}(t_4 - t_3) = 0 \tag{25}$$

Substituting (17), (19) and (23) into (25), the following equation can be found.

$$kD(V_{in} + V_c) = \frac{V_o}{n}(1 - D) \tag{26}$$

If the leakage inductances of the transformers are neglected, the coupling-coefficient k is equal to 1. In additon, the voltage V_c can be written as:

$$V_c = \frac{V_o}{n} \tag{27}$$

Substituting (27) and k = 1 into (26), the voltage gain of the proposed converter is found as follows:

$$M = \frac{V_o}{V_{in}} = \frac{I_{in}}{I_o} = \frac{nD}{1 - 2D} \tag{28}$$

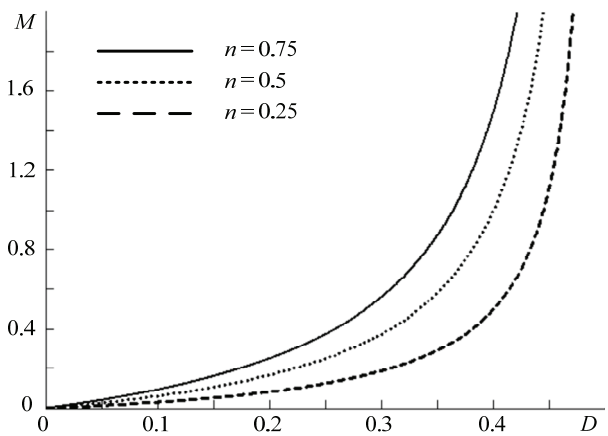

Fig. 5. Voltage gain of the proposed converter under different turns ratios.

From the above equation, it can be seen that the duty ratio D cannot be larger than 0.5. Fig. 5 displays curve of the voltage gain M under different turns ratios.

B. Boundary Operating Condition

For the sake of simplicity, the leakage inductance of the transformer ignored. When the proposed converter is operated in the boundary conduction mode, the peak value of the magnetizing-inductance current can be found from (18).

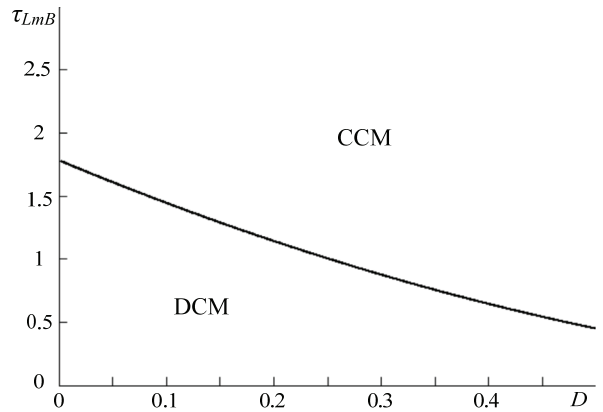

Fig. 6. Boundary condition of the proposed converter at n = 0.75.

$$I_{Lmp} = \frac{V_{in} + V_c}{L_m} DT_s = \frac{nV_{in} + V_o}{nL_m} DT_s \tag{29}$$

The average value of the output-capacitor current can be written as:

$$I_{co} = \frac{I_{Lmp}}{n}(1-D) - I_o \tag{30}$$

Using the ampere-second balance principle for the output capacitor, it can be seen that the average value of the output-capacitor current I_{co} is equal to 0. Therefore:

$$\frac{I_{Lmp}}{n}(1-D) = I_o = \frac{V_o}{R} \tag{31}$$

The magnetizing-inductance time constant is defined as:

$$\tau_{Lm} \equiv \frac{L_m}{RT_s} \tag{32}$$

Using (28)-(29) and (31)-(32), the boundary magnetizing-inductance time constant τ_{LmB} is derived as:

$$\tau_{LmB} = \frac{(1-D)^2}{n^2} \tag{33}$$

A curve of the boundary magnetizing-inductance time constant τ_{LmB} is plotted in Fig. 6. At $\tau_{Lm} > \tau_{LmB}$, the proposed converter is operated in the CCM.

C. Voltage Stresses on the Power Devices

From the operating principle analysis, the voltage stresses on the active switch S_1 and the diodes D_1, D_2, D_3 are given as:

$$V_{S1} = V_{D1} = V_{in} + \frac{2V_o}{n} \tag{34}$$

$$V_{D2} = V_{D3} = nV_{in} + 2V_o \tag{35}$$

D. Power Losses Analysis

The average of the input current is written as:

$$I_{in(av)} = \frac{nD}{1-2D} I_o \tag{36}$$

During the switch S_1 ON-period, the average and root-mean-square of the switch-current are derived as:

$$I_{S1(av)} = \frac{n}{1-2D} I_o \tag{37}$$

$$I_{S1(rms)} = \frac{n\sqrt{D}}{1-2D} I_o \tag{38}$$

Thus, the power loss of the switch S_1 is given as follows:

$$P_{S1} = I_{S1(rms)}^2 r_{S1} = \frac{n^2 D}{(1-2D)^2} I_o^2 r_{S1} \tag{39}$$

where r_{S1} is the ON-state resistance of the switch S_1. The average of the capacitor-current are given as:

$$I_{c1(av)} = I_{c2(av)} = \begin{cases} -\dfrac{I_{S1(av)}}{2}, & S_1 \text{ ON} \\ \dfrac{D}{2(1-D)} I_{S1(av)}, & S_1 \text{ OFF} \end{cases} \tag{40}$$

$$I_{co(av)} = \begin{cases} -I_o, & S_1 \text{ ON} \\ \dfrac{D}{1-D} I_o, & S_1 \text{ OFF} \end{cases} \tag{41}$$

The root-mean-square of the capacitor-current is derived as:

$$I_{c1(rms)} = I_{c2(rms)} = \frac{I_{S1(av)}}{2}\sqrt{\frac{D}{1-D}} = \frac{nI_o}{2(1-2D)}\sqrt{\frac{D}{1-D}} \tag{42}$$

$$I_{co(rms)} = \sqrt{\frac{D}{1-D}} I_o \tag{43}$$

Therefore, the power losses of the capacitors are written as:

$$P_{c1} = P_{c2} = I_{c1(rms)}^2 r_{c1} = \frac{n^2 D}{4(1-D)(1-2D)^2} I_o^2 r_{c1} \tag{44}$$

$$P_{co} = I_{co(rms)}^2 r_{co} = \frac{D}{1-D} I_o^2 r_{co} \tag{45}$$

where r_{c1} and r_{co} are the ESRs of the capacitors C_1 and C_o. During the switch S_1 OFF-period, the average of the diode-current is derived as:

$$I_{D1(av)} = \frac{D}{1-D} I_{S1(av)} = \frac{nD}{(1-D)(1-2D)} I_o \tag{46}$$

$$I_{D2(av)} = I_{D3(av)} = \frac{1}{2(1-D)} I_o \tag{47}$$

$$I_{D2(rms)} = I_{D3(rms)} = \frac{1}{2\sqrt{1-D}} I_o \tag{48}$$

Thus, the power losses of the diodes D_1-D_3 in the ON-state forward voltage-drop are found as follows:

$$P_{D1} = V_{FD1} I_{D1(av)} = \frac{nDV_{FD1} I_o}{(1-D)(1-2D)} \tag{49}$$

$$P_{D2} = P_{D3} = V_{FD2} I_{D2(av)} = \frac{V_{FD2} I_o}{2(1-D)} \tag{50}$$

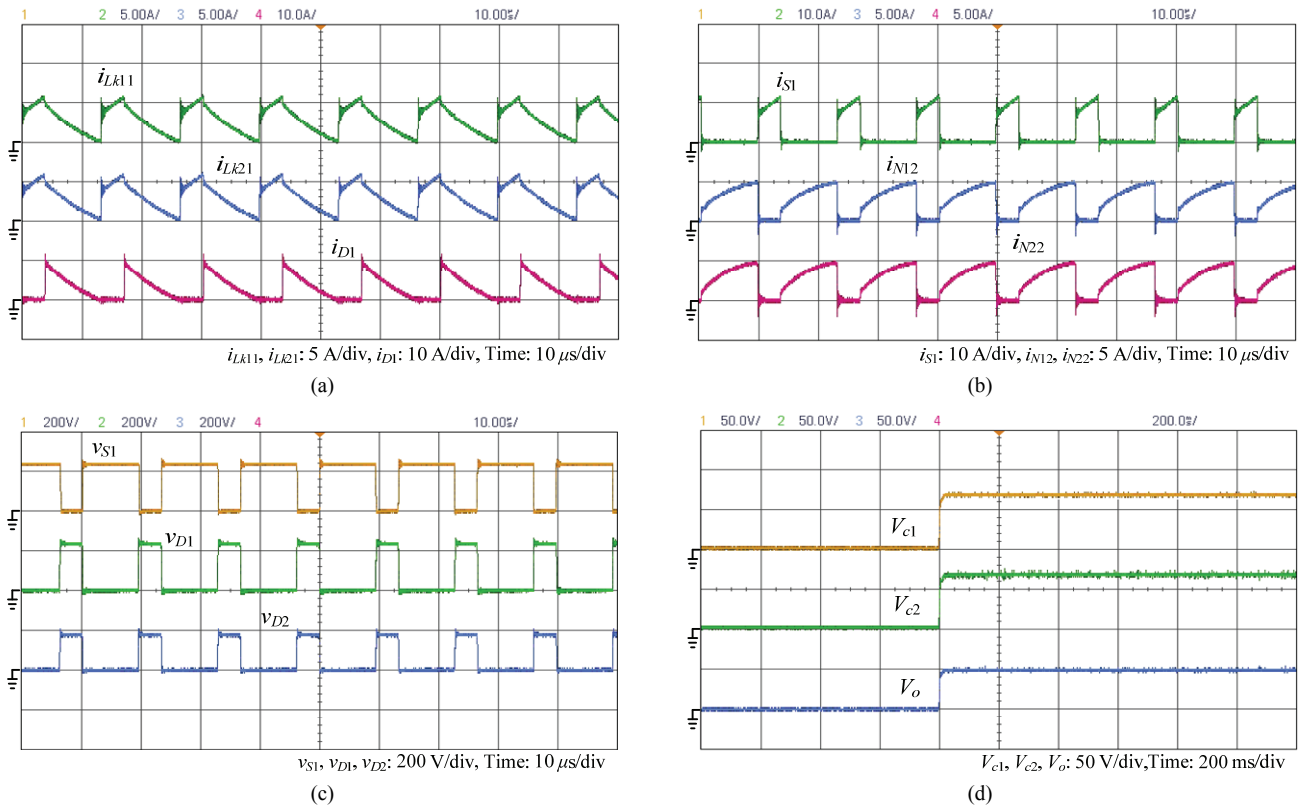

Fig. 7. Experimental waveforms under V_{in} = 100 V, V_o = 48 V and P_o = 250 W: (a) i_{Lk11}, i_{Lk21} and i_{D1}; (b) i_{S1}, i_{N12} and i_{N22}; (c) v_{S1}, v_{D1} and v_{D2}; (d) V_{c1}, V_{c2} and V_o.

where V_{FD1} and V_{FD2} are the ON-state forward voltage-drop of the diodes D_1 and D_2. The average of the leakage-inductor currents of the transformers TR_1 and TR_2 are given as:

$$I_{Lk11(av)} = I_{Lk21(av)} = \begin{cases} \dfrac{I_{S1(av)}}{2}, & S_1 \text{ ON} \\ \dfrac{D}{2(1-D)} I_{S1(av)}, & S_1 \text{ OFF} \end{cases} \quad (51)$$

The root-mean-square of the leakage-inductor currents of TR_1 and TR_2 are derived as:

$$I_{Lk11(rms)} = I_{Lk21(rms)} = \frac{nI_o}{2(1-2D)}\sqrt{\frac{D}{1-D}} \quad (52)$$

Thus, the power losses of the primary-winding of TR_1 and TR_2 are given as:

$$P_{11} = P_{21} = I_{Lk11(rms)}^2 r_{11} = \frac{n^2 D}{4(1-D)(1-2D)^2} I_o^2 r_{11} \quad (53)$$

where r_{11} is the ESR of the primary winding of TR_1. The power losses of the secondary-winding of TR_1 and TR_2 are obtained as:

$$P_{12} = P_{22} = I_{D2(rms)}^2 r_{12} = \frac{I_o^2 r_{12}}{4(1-D)} \quad (54)$$

where r_{12} is the ESR of the secondary winding of TR_1.

IV. Experimental Results

A prototype circuit has been built in the laboratory to verify the feasibility of the proposed converter. The circuit specifications and components are selected as input voltage V_{in} = 100 V, output voltage V_o = 48 V, output power P_o = 250 W, switching frequency f_s = 75 kHz, capacitors $C_1 = C_2$ = 100 μF and C_o = 470 μF, turn-ratio of the transformers n = 0.75, switch S_1 IXTQ52N30P, and diodes D_1, D_2 and D_3: STTH6003CW. Thus, the voltage gain M is equal to 0.48. Substituting the voltage gain M = 0.48 and the turns ratio n = 0.75 into (28), the duty ratio D is found to be 0.28. Substituting the turns ratio n = 0.75 and the duty ratio D = 0.28 into (33), the boundary magnetizing-inductance time constant τ_{LmB} is derived as 0.92. It is assumed that the proposed converter is operated in the CCM from 40% of the full load. Thus, the load R is 23 Ω. At $\tau_{Lm} > \tau_{LmB}$, the proposed converter is operated in the CCM. Therefore:

$$L_m > \tau_{LmB} R T_s = 0.92 \times 23 \times 13.3\mu = 281\ \mu\text{H} \quad (55)$$

The magnetizing-inductance L_m is selected as 285 μH.

Under input voltage V_{in} = 100 V, output voltage V_o = 48 V and output power P_o = 250 W, some experimental waveforms are shown in Fig. 7. Fig. 7(a) shows waveforms of i_{Lk11}, i_{Lk21} and i_{D1}. It can be seen that the waveforms i_{Lk11} and i_{Lk21} are almost same. In addition, the summation of the currents i_{Lk11}

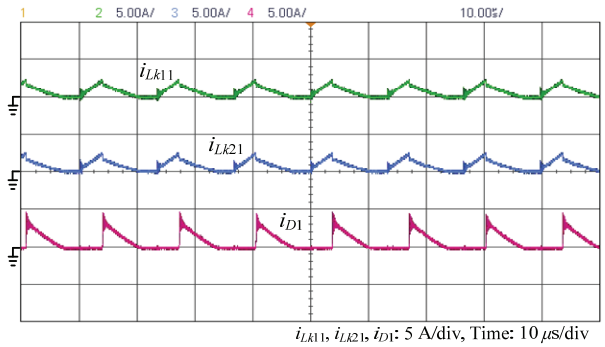

Fig. 8. Experimental waveforms of i_{Lk11}, i_{Lk21} and i_{D1} under V_{in} = 100 V, V_o = 48 V and P_o = 70 W.

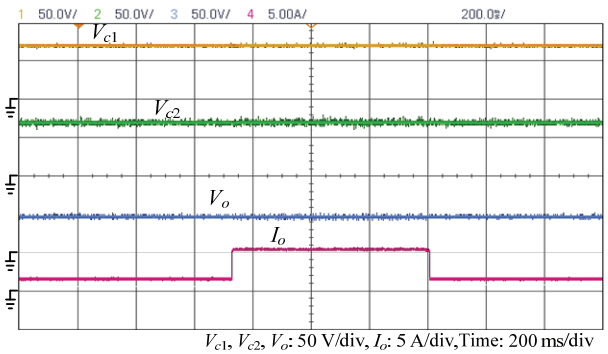

Fig. 9. Dynamic response of the proposed converter for a load change between 70W and 250W.

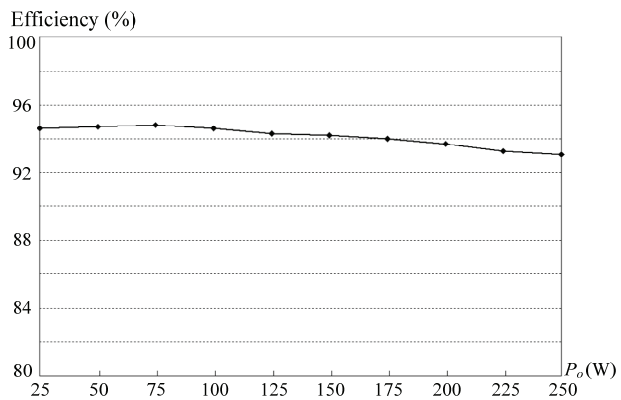

Fig. 10. Measured efficiency at various output powers.

and i_{Lk21} is equal to the current i_{D1} during the switch S_1 OFF-period. Thus, it can be ensured that the leakage energies of the transformers can be recycled to the capacitors C_1 and C_2 via the diode D_1. Fig. 7(b) shows the waveforms i_{S1}, i_{N12} and i_{N22}. It can be seen that the summation of the currents i_{Lk11} and i_{Lk21} is equal to the current i_{S1} during the switch S_1 ON-period. Fig. 7(c) shows waveforms of v_{S1}, v_{D1} and v_{D2}, which agree with the operating principle and steady-state analysis. Fig. 7(d) shows waveforms of V_{c1}, V_{c2}, and V_o in the start-up process. It can be seen that the voltage V_o is controlled at the setting value. Fig. 8 shows experimental waveforms under V_{in} = 100 V, V_o = 48 V and P_o = 70 W. The load R and the magnetizing-inductance time constant τ_{Lm} are 33 Ω and 0.648, respectively. Thus, τ_{Lm} is less than τ_{LmB}. It can be seen that the proposed converter is operated in the discontinuous conduction mode. Fig. 9 shows the dynamic response of the proposed converter for a load change between 70W and 250W. Fig. 10 shows the measured efficiency of this prototype circuit. The maximum measured efficiency is 94.8% and the measured efficiency is 93.1% under the full-load condition.

V. Conclusions

The conventional DC-DC flyback converter has the merits of a simple structure and low cost. However, this converter also possesses leakage inductance of the transformer. This results in a lower efficiency. In this paper, only a single switch is used in the proposed converter. This proposed converter employs two transformers with the same inductance. During the switch OFF-period, the energies of the magnetizing-inductance of the transformers are released to the output. Meanwhile, the leakage energies of the transformers can be recycled. From the obtained experimental results, it can be seen that the leakage energies of the transformers have been recycled. In addition, the measured efficiency is 93.1% under the full-load condition and the maximum efficiency is 94.8%.

References

[1] F. Marvi, E. Adib, and H. Farzanehfard, "Efficient ZVS synchronous buck converter with extended duty cycle and low-current ripple," *IEEE Trans. Ind. Electron.*, Vol. 63, No. 9, pp. 5403-5409, Sep. 2016.

[2] W. Hu, F. Zhang, X. Long, X. Chen, and W. Deng, "Stability analysis and control of nonlinear behavior in V2 switching buck converter," *J. Power Electron.*, Vol. 14, No. 6, pp. 1208-1216, Nov. 2014.

[3] V. I. Kumar and S. Kapat, "Unified digital current mode control tuning with near optimal recovery in a CCM buck converter," *IEEE Trans. Power Electron.*, Vol. 31, No. 12, pp. 8461-8470, Dec. 2016.

[4] Y. X. Wang, D. H. Yu, and Y. B. Kim, "Robust time-delay control for the DC-DC boost converter," *IEEE Trans. Ind. Electron.*, Vol. 61, No. 9, pp. 4829-4837, Sep. 2014.

[5] W. J. Choi, S. K. Kim, J. Kim, and K. B. Lee, "Input-constrained current controller for DC/DC boost converter," *J. Power Electron.*, Vol. 16, No. 6, pp. 2016-2023, Nov. 2016.

[6] M. L. Nejad, B. Poorali, E. Adib, and A. A. M. Birjandi, "New cascade boost converter with reduced losses," *IET Power Electron.*, Vol. 9, No. 6, pp. 1213-1219, May 2016.

[7] C. Yao, X. Ruan, W. Cao, and P. Chen, "A two-mode control scheme with input voltage feed-forward for the two-switch buck-boost DC-DC converter," *IEEE Trans. Power Electron.*, Vol. 29, No. 4, pp. 2037-2048, Apr. 2014.

[8] S. Miao, F. Wang, and X. Ma, "A new transformerless buck-boost converter with positive output voltage," *IEEE Trans. Ind. Electron.*, Vol. 63, No. 5, pp. 2965-2975, May 2016.

[9] P. Deivasundari, G. Uma, and S. Ashita, "Chaotic dynamics of a zero average dynamics controlled DC-DC Cuk converter," *IET Power Electron.*, Vol. 7, No. 2, pp. 289-298, Feb. 2014.
[10] Z. Chen, "PI and sliding mode control of a Cuk converter," *IEEE Trans. Power Electron.*, Vol. 27, No. 8, pp. 3695-3703, Aug. 2012.
[11] N. Pragallapati and V. Agarwal, "Distributed PV power extraction based on a modified interleaved SEPIC for nonuniform irradiation conditions," *IEEE J. Photovolt.*, Vol. 5, No. 5, pp. 1442-1453, Sep. 2015.
[12] E. Babaei and M. E. S. Mahmoodieh, "Calculation of output voltage ripple and design considerations of SEPIC converter," *IEEE Trans. Ind. Electron.* Vol. 61, No. 3, pp. 1213-1222, Mar. 2014.
[13] H. Wu, P. Xu, W. Liu, and Y. Xing, "Series-input interleaved forward converter with a shared switching leg for wide input voltage range applications," *IEEE Trans. Ind. Electron.*, Vol. 60, No. 11, pp. 5029-5039, Nov. 2013.
[14] J. Yuan Lin, P. J, Liu, and C. Y. Yang, "A dual-transformer active-clamp forward converter with nonlinear conversion ratio," *IEEE Trans. Power Electron.*, Vol. 31, No. 6, pp. 4353-4361, Jun. 2016.
[15] K. B. Park, G. W. Moon, and M. J. Youn, "Two-switch active-clamp forward converter with one clamp diode and delayed turnoff gate signal," *IEEE Trans. Ind. Electron.*, Vol. 58, No. 10, pp. 4768-4772, Oct. 2011.
[16] P. Thummala, H. Schneider, Z. Zhang, Z. Ouyang, A. Knott, and M. A. E. Andersen, "Efficiency optimization by considering the high-voltage flyback transformer parasitics using an automatic winding layout technique," *IEEE Trans. Power Electron.*, Vol. 30, No. 10, pp. 5755-5768, Oct. 2015.
[17] G. M. L. Chu, D. D. C. Lu, and V. G. Agelidis, "Practical application of valley current mode control in a flyback converter with a large duty cycle," *IET Power Electron.*, Vol. 5, No. 5, pp. 552-560, May 2012.
[18] A. Fernandez, J. Sebastian, P. J. Villegas, M. M. Hernando, and L. A. Barcia, "Low-power flyback converter with synchronous rectification for a system with AC power distribution," *IEEE Trans. Ind. Electron.*, Vol. 49, No. 3, pp. 598-606, Jun. 2002.
[19] C. O. Yeon, J. B. Lee, I. O. Lee, and G. W. Moon, "Wide ZVS range asymmetric half-bridge converter with clamp switch and diode for high conversion efficiency," *IEEE Trans. Ind. Electron.*, Vol. 63, No. 5, pp. 2862-2870, May 2016.
[20] M. Arias, M. F. Diaz, J. E. R. Cadierno, D. G. Lamar, and J. Sebastian, "Digital implementation of the feedforward loop of the asymmetrical half-bridge converter for LED lighting applications," *IEEE J. Emerg. Sel. Topics Power Electron.*, Vol. 3, No. 3, pp. 642-653, Sep. 2015.
[21] S. W. Choi, J. M. Lee, and J. Y. Lee, "High-efficiency portable welding machine based on full-bridge converter with ISOP-connected single transformer and active snubber," *IEEE Trans. Ind. Electron.*, Vol. 63, No. 8, pp. 4868-4877, Aug. 2016.
[22] W. J. Cha, J. M. Kwon, and B. H. Kwon, "Highly efficient asymmetrical PWM full-bridge converter for renewable energy sources," *IEEE Trans. Ind. Electron.*, Vol. 63, No. 5, pp. 2945-2953, May 2016.
[23] P. Xuewei and A. K. Rathore, "Current-fed soft-switching push-pull front-end converter-based bidirectional inverter for residential photovoltaic power pystem," *IEEE Trans. Power Electron*., Vol. 29, No. 11, pp. 6041-6051, Nov. 2014.
[24] K. R. Sree and A. K. Rathore, "Impulse commutated zero-current switching current-fed push-pull converter: analysis, design, and experimental results," *IEEE Trans. Ind. Electron.*, Vol. 62, No. 1, pp. 363-370, Jan. 2015.
[25] S. J. Finney, B. W. Williams, and T. C. Green, "RCD snubber revisited," *IEEE Trans. Ind. Appl.*, Vol. 32, No. 1, pp. 155-160, Jan./Feb. 1996.
[26] M. G. Kim and Y. S. Jung, "A novel soft-switching two-switch flyback converter with a wide operating range and regenerative clamping," *J. Power Electron.*, Vol. 9, No. 5, pp. 772-780, Sep. 2009.
[27] D. M. Bellur and M. K. Kazimierczuk, "Zero-current-transition two-switch flyback pulse-width modulated DC-DC converter," *IET Power Electron.*, Vol. 4, No. 3, pp. 288-295, Mar. 2011.
[28] G. Spiazzi, P. Mattavelli, and A. Costabeber, "High step-up ratio flyback converter with active clamp and voltage multiplier," *IEEE Trans. Power Electron.*, Vol. 26, No. 11, pp. 3205-3214, Nov. 2011.
[29] G. Chen, Y. S. Lee, S. Y. R. Hui, D. Xu, and Y. Wang, "Actively clamped bidirectional flyback converter," *IEEE Trans. Ind. Electron.*, Vol. 47, No. 4, pp. 770-779, Aug. 2000.
[30] T. J. Liang, W. Y. Huang, L. S. Yang, S. M. Chen, and J. F. Chen, "Interleaved Flyback Converter Device with Leakage Energy Recycling," UA Patent, No. US 8374000 B2, Feb. 2013.

Lung-Sheng Yang was born in Taiwan, ROC, in 1967. He received his B.S. degree in Electrical Engineering from the National Taiwan Institute of Technology, Taipei, Taiwan, in 1990; his M.S. degree in Electrical Engineering from the National Tsing-Hua University, Hsinchu, Taiwan, in 1992; and his Ph.D. degree in Electrical Engineering from the National Cheng Kung University, Tainan, Taiwan, in 2007. He is presently working as an Associate Professor in the Department of Electrical Engineering, Far East University, Tainan, Taiwan. His current research interests include power factor correction, dc-dc converters, renewable energy conversion and electronic ballasts.